Water Modeling the Solid Oxide Membrane Electrolysis with Rotating Cathode Process

By

Chris Kinney

Submitted to the Department of Materials Science
and Engineering in Partial Fulfillment of the Requirements for the
Degree of

Bachelor of Science

At the

Massachusetts Institute of Technology

June 2004

Signature of Author ....
Department of Materials Science and Engineering
May 6th, 2004

Certified by..
Adam Powell
Assistant Professor of Materials Engineering
Thesis Supervisor

Accepted by..
Lorna J. Gibson
Matoula S. Salapatas Professor of Materials Science and Engineering
Chairman, Undergraduate Thesis Committee

Abstract

The Kroll process for refining titanium is an expensive batch process which produces a final product that still requires intensive post processing to create usable titanium. A new process, Solid Oxide Membrane Electrolysis with Rotating Cathode (SOMERC) process is being explored. The SOMERC process is a continuous process that could produce large quantities of high quality titanium at a fraction of the cost of the Kroll process. This paper examines the fluid flow around the ingot in the SOMERC Process. A large shear between the ingot and surrounding fluid will create a fully-dense ingot instead of dendrites, because dendrites are undesirable. Using a camera, a plane of light and titanium dioxide particles, videos and pictures of the water were taken and analyzed to find how to create a large amount of shear between the ingot and the fluid. Out of the speeds tested, a rotation rate of 900°/s for the ingot proved to create the most shear, and therefore the shear between the ingot and fluid increases with increasing rotation rate, making it more likely to suppress the formation of dendrites.

Table of Contents

List of Figures and Tables

Introduction:

In recent years, the demand for titanium has skyrocketed. Given titanium's success in the motorcycle and aerospace market, car companies are now planning to place titanium alloys in suspension springs. In just the motorcycle exhaust system market, demand for titanium and its alloys has gone from 20 metric tons in 1997 up approximately 3000% in just 5 years, to 600 metric tons in 2002.[1] These increases in the demand for titanium are driving research to find a cheaper, easier way to make titanium. The work done in this thesis will contribute to finding a new way to make titanium.

Titanium and its alloys have a high strength to weight ratio, fracture toughness, ductility, high corrosion resistance and many other highly desirable qualities. Yet the current primary way of making titanium, the Kroll process, is expensive and fairly complex. The Kroll process is a multi-step process. In the first step, titanium tetrachloride is sprayed onto a hot and highly reactive surface where it reacts and forms a sponge. In the second stage, the sponge is chopped up into small chips, which are acid-leached, water-washed and then dried. In the third stage, the chips are compressed and then made into an electrode, which is then melted into an ingot. The Kroll process has several disadvantages including the fact that it is a multi step process where each step is a separate batch, and it is very hard to remove all the impurities in the titanium.[2]

Some of the more specific disadvantages of the Kroll process are that it requires pure $TiCl_4$, which must be produced separately from the naturally occurring

---

[1] Faller, "Titanium alloy to be placed in Japanese automobiles" (Advanced Materials and Processes 160, no. 1), 15

[2] Crowley, "How to Extract Low-Cost Titanium" (Advanced Materials and Processes 161, no. 11), 27

ore, and deals with chlorine, which has health, safety and environmental concerns. Another problem intrinsic to batch processes is that the optimal reaction rates are only reached in a fraction of the overall process cycle time. The Kroll process takes approximately 85 hours, and the reaction is at its maximum rate for only 1/3 of the cycle. The final product of the Kroll process is a porous, sponge titanium, which contains a decent amount of chlorine trapped as small chloride inclusions in the porous titanium. Therefore the titanium must be ground into chips, acid leached, washed and dried. The chips are compressed into electrodes which then are formed into an ingot through vacuum arc remelting.[3]

In addition to chloride inclusions, the sponge titanium can also have titanium nitride inclusions. These inclusions are hard to detect before the vacuum arc remelting. Since the inclusions are hard and brittle, it is extremely bad if they are present in the final product, because they could be nucleation points for failure in the material. To remove the inclusions, which can not be filtered out, the titanium is vacuum arc remelted 3 times. Newer methods such as electron beam cold hearth melting and plasma arc melting are beginning to be used because they are better at removing the nitride than the triple VAR.[4] Regardless, all of these steps add cost to the final product.

Currently there is work being done to make titanium using a modified Czochralski process. The Czochralski process for growing silicon crystals involves a rotating crucible of molten silicon. A seed crystal is placed in the center, which is then rotated in the opposite direction as the crucible. As the seed is rotating, it is

---

[3] Kirchain, Randolph. *The role of Titanium in the Automobile: Understanding the Economic Implications of Three Emerging Technologies*. Technical Report, Camanoe Associates, USA, July 2002.
[4] Ibid

withdrawn from the melt, creating a silicon ingot. By controlling the temperature and rotating speeds of the seed and crucible, an exact diameter can be produced for the ingot, which generally ranges from 1 to 2 meters in length.

The modified Czochralski process is more officially known as the Solid Oxide Membrane Electrolysis with Rotating Cathode (SOMERC) process. It is a process where a rotating titanium cathode is withdrawn from the crucible as titanium plates onto it. There are several solid oxide membrane (SOM) encased anodes surrounding the cathode around an outer circumference. Between the SOM anodes and the titanium cathode is a semi-permeable barrier in the shape of a cylindrical shell. The barrier controls the flow between the inner area where the cathode is rotating quickly and the outer area where the moderately fragile SOM anodes reside. The barrier can also act as a second cathode, which will reduce the more electronegative impurities like iron and nickel. By keeping the barrier at a slightly lower voltage difference (the voltage difference between the barrier and anodes is less than the difference between the cathode and anodes), the impurities will not get through the barrier. This will keep the titanium in the inner crucible pure. A schematic of the SOMERC process and the SOM electrolytes / anodes can be seen in figure 1.[5]

[5]A. Powell, "Solid Oxide Membrane Electrolysis with Rotating Cathode (SOMERC), a Low-Cost Process for Commercial-Purity Dense Titanium," MIT Technology Licensing Office Disclosure Report, January 9, 2003.

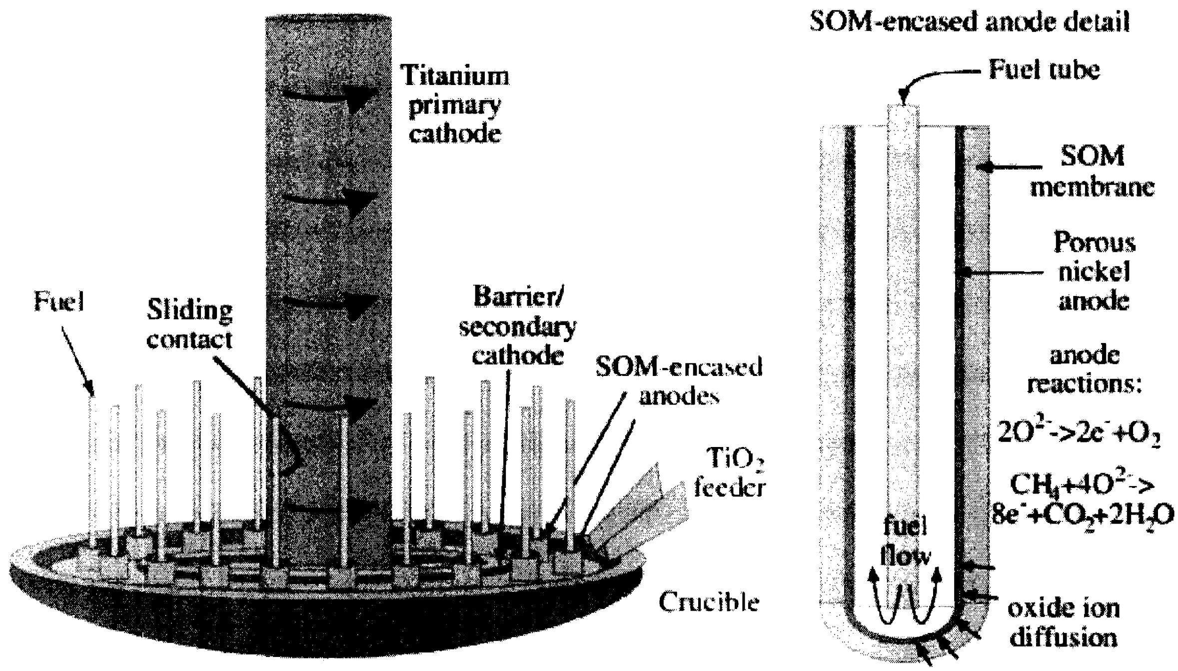

Figure 1: The SOMERC Process. Certain elements are represented yet not shown in their entirety; there will be multiple TiO_2 feeders and sliding contacts.[6]

One of the problems with most titanium electrolysis processes is ion cycling. In titanium electrolytic refining cells, Ti^{3+} ions are reduced to Ti^{2+} ions at the cathodes. However, as the process continues on, Ti^{3+} ions crowd around the cathode, preventing more reduction. The Ti^{2+} ions can then work their way back to the anode, give up an electron and become Ti^{3+} ions again. This can reduce the efficiency of the titanium electrolysis by up to 70%. However, the SOM anode, which has yttria-stabilized zirconia (YSZ) as the solid metal oxide, avoids this problem. YSZ is a good conductor of oxide ions but a poor conductor of electrons, so Ti^{2+} will not give up its electron. By using the SOM electrolyte / anode, the ion cycling problem found in most titanium electrolysis is eliminated from the SOMERC process.

[6] Ibid.

Another concern about the SOMERC process is the possibility of dendrites growing on the cathode. Small non-uniformities on the surface of the cathode can grow into dendrites due to a Mullins-Sekerka instability. This instability arises near the perturbation because the diffusion boundary layer is thinner and the electric field is stronger by the non-uniformity than in the immediate vicinity. The thinner diffusion layer and stronger electric field cause ions to diffuse faster and plate onto the metal more quickly there, making the perturbation grow into a dendrite. This problem can be avoided if there is a high shear flow across the surface of the ingot. The high shear flow will cause the non-uniformities to shift and decay away. Merton Fleming's research group at MIT has discovered that under high enough shear, solid metal nuclei can grow as spheroids that are free of dendrites.[7] Hopefully dendrite formation can be suppressed if there is a high enough shear across the sides and bottom of the titanium cathode.

As the titanium cathode grows, there will be more and more internal electrical resistance, simply because there is more material for the current to travel through. There are two ways to keep the voltage across the electrochemical cell constant, one being to increase the total voltage as the internal resistance increases so that the voltage at the surface remains constant. Another possibility is to use sliding contacts, which can be seen in the schematic in figure 1. These contacts may reduce the inefficiency of Joule heating (employed to keep the melt molten). Care must also be taken to ensure that the contacts are not too low on the ingot, because they could increase the electric field at the outer edge of the cathode-flux interface.

[7] Merton Flemings, Raul A. Martinez, private conversation

This paper will look at a specific aspect of the SOMERC processes. It will examine the velocities of tracer particles dropped into a water model of the SOMERC process. Understanding the velocities (angular, radial and in the z direction) will help create a more complete picture of the SOMERC Process, so that the process can be better understood and analyzed.

Equipment:

The water tank was the first acquisition along the road to building a model of a Czochralski process. The tank measures approximately 43" by 46" and is about 10" tall. The tank is made of plexiglass; a silicone based bathroom sealant caulk was used around all the joints of the tank to ensure that it is watertight. To ensure that the water tank will accurately model the flow of the titanium flux in the crucible, Reynolds, Weber and Froude numbers were compared (all three are dimensionless numbers). The Reynolds number is shown in equation 1. The Reynolds number represents the ratio of inertial to viscous forces. The Weber number is shown in equation 2, and is the ratio of inertial to surface tension forces. By matching the Reynolds and Weber numbers of the water tank as well as the SOMERC process, it allows the assumption that the surface tension and viscosity characteristics of the melt will be accurately represented by the water tank. The Froude number is shown in equation 3, by controlling the velocity and size, one can match two of these three dimensionless numbers to the real process.

$$\mathrm{Re} = \frac{\rho V L}{\eta} \qquad \text{(eq. 1)}$$

$$W = \frac{\rho V^2 L}{\sigma} \qquad \text{(eq. 2)}$$

$$FR = \frac{V^2}{GL} \qquad \text{(eq. 3)}$$

Equations 1-3, with density (ρ), velocity (V), length scale (L), viscosity (η), surface tension (σ), and the gravitational constant ($G = 9.8\ m/s^2$)

The Reynolds and Weber numbers were calculated for SOMERC process and then compared in a large table to the possible sizes and velocities that would be present in the water tank. The numbers that agreed well with each other were then checked with the Froude number. The tank is an appropriate size for the speeds that the ingot will be rotated at, which is between 1 and 5 revolutions per second.

The next step in constructing the model is rotating the ingot. To rotate the ingot, a variable speed drill is mounted above the tank on a platform. The drill platform is elevated above the tank with four 2"-by-4" posts. The platform consists of two parallel plywood sheets separated and attached by 2"-by-4" posts on their side (the separation between the two plywood sheets is 1.5", see figure 2). The plywood sheets have holes in them that are aligned to keep the shaft straight up and down.

Figure 2. The gap between the plywood sheets which aligns the shaft. There are multiple sets of holes drilled through the sheet to allow for different placements of the shaft and ingot.

The shaft is a 3/8" threaded rod approximately 2 feet long. The shaft is connected to the drive shaft of a variable speed drill; and the drill's cover is removed so that the speed of the drill can be set and maintained throughout an experiment. The drill is mounted sideways on another plywood sheet, which is then attached with L-brackets to the top of the two parallel plywood sheets. (see figure 3.)

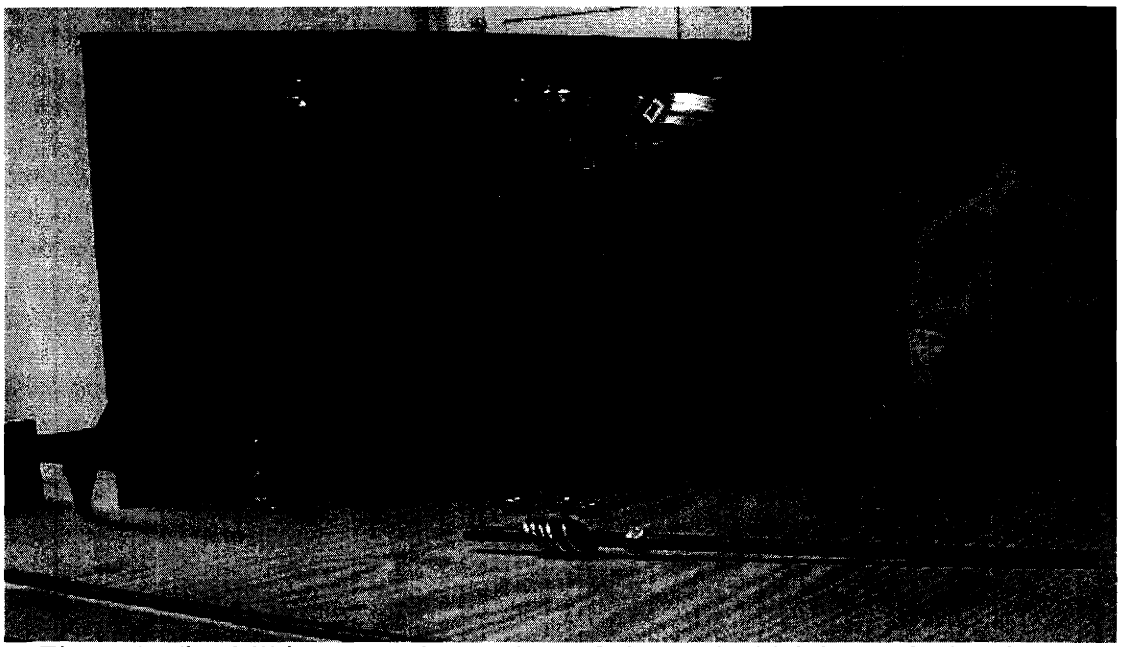

Figure 3. The drill is mounted on a piece of plywood which is attached to the top sheet of the two parallel sheets seen in figure 2.

The ingot can be attached on the end of the shaft. Using a nut, then a washer on the bottom and a nut on the top, the top cap of the ingot can be stabilized at a desired height. Loctite or a similar compound can be applied to the nuts and the rod so that they do not shake loose as the shaft spins. The pvc pipe that serves as the ingot can then be attached to the top cap that is already attached to the shaft. The tank can then be filled up to any height depending on the specific experiment (see figure 4).

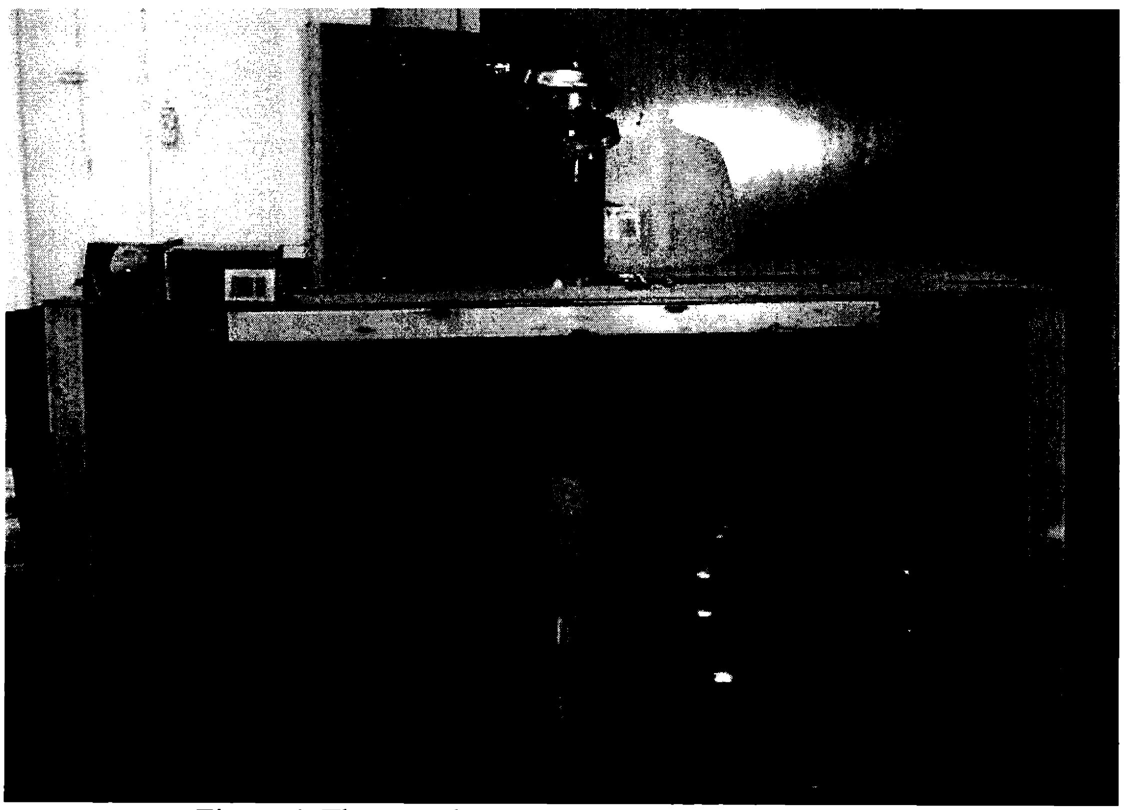

Figure 4. The complete set up, without water in the tank.

The setup allows for flexibility in that different sizes of pvc pipe can be attached to the shaft to simulate different ingot sizes. Also, there are more alignment holes drilled in the top of the parallel plywood sheets. Therefore, using a belt drive system, a belt can be driven off the center shaft and spin the outer shafts, each with their own ingot attached. More alignment holes can be drilled as well, allowing for a setup that is easily tailored to test a specific aspect of the water interacting with multiple ingots.

In order to estimate the flow velocity distribution, titanium dioxide particles are dropped into the water. With all the lights turned off, a plane of light is projected through the water; illuminating the titanium dioxide particles. By using a camera with a long shutter speed, a picture of the paths of the particles can be taken and the path of the water flow can be seen. The plane of light is created by enclosing a halogen bulb in a cardboard box. The light is held upright in the box by its fixture; and a slit is cut in the box on the same level as the filament. The inside of the box is covered in aluminum foil to reflect both the light and heat given off by the halogen bulb.

Using a Canon Optura 300 video camera, video is taken of the particles' flow. As the TiO_2 particles pass through the plane of light, they illuminate and their path can be seen. Once the video has been recorded, it is imported into Adobe Premiere, a video editing program. First, clips which clearly show the particles are selected; then a frame within the clip is exported to a picture file. Then, the picture file is then used in conjunction with the video clip to draw the paths of the particles on the picture. The pvc ingot can be seen in all the clips, providing a length scale in the picture. The video file has a timeline associated with it, so it is possible to find the distance the particle traveled over a certain length of time, which will provide a rough velocity of the particle.

Once the pictures have been taken, they can be analyzed. Simulating the flows of the Czochralski crystal growth process can be very computationally intensive. Several methods have been used to model the flows, including a low-order finite difference method, and a finite volume method. The low-order methods are accurate, but require a lot of grid points. Since the low-order methods need a lot of grid points, those methods consume a large amount of processing time and virtual memory. However, the generalized differential quadrature (GDQ) method gives accurate results and uses a much smaller number of grid points, which means it requires much less computational power.[8]

The GDQ method approximates the spatial derivative at a certain point using a linear weighted sum of all the functional values in the domain. The weighted coefficients for the first-order derivatives are calculated by using an algebraic formula. There are no restrictions on the choice of grid points, and the coefficients of the second, third and higher order derivatives are calculated through a recurrence relationship. The GDQ method has been used with very few grid points to accurately solve flow problems while only using a small amount of processor time and virtual storage.[9]

The weighting coefficients are calculated by analyzing a high-order polynomial approximation as well as linear-vector space. Once the grid points are known, the coefficients for the first order derivative can be calculated using equations 4-9 below[10].

---

[8] Chew, "An efficient approach for numerical simulation of flows in Czochralski crystal growth" (Journal of Crystal Growth 181, no. 1), 427
[9] Ibid, 428
[10] Ibid, 428-429

$$f_x^{(n)}(x_i, y_j) = \sum_{k=1}^{N} w_{ik}^{(n)} f(x_k, y_j),\ n = 1,2,\dots,\ N-1 \qquad \text{(eq. 4)}$$

$$f_y^{(m)}(x_i, y_j) = \sum_{k=1}^{M} \bar{w}_{jk}^{(m)} f(x_i, y_k),\ m = 1,2,\dots,\ M-1 \qquad \text{(eq. 5)}$$

$$w_{ij}^{(1)} = \begin{cases} \dfrac{A^{(1)}(x_i)}{(x_i - x_j) A^{(1)}(x_j)}, & i \neq j \\ -\displaystyle\sum_{k=1, k\neq i}^{N} w_{ik}^{(1)}, & i = j \end{cases} \qquad \text{(eq. 6)}$$

$i, j = 1, 2, \dots, N$,

$$\bar{w}_{ij}^{(1)} = \begin{cases} \dfrac{B^{(1)}(y_i)}{(y_i - y_j) B^{(1)}(y_j)}, & i \neq j \\ -\displaystyle\sum_{k=1, k\neq i}^{M} \bar{w}_{ik}^{(1)}, & i = j \end{cases} \qquad \text{(eq. 7)}$$

$i, j = 1, 2, \dots, M$,

where

$$A^{(i)}(x_i) = \prod_{j=1, j\neq i}^{N} (x_i - x_j), \quad \text{and} \quad B^{(i)}(y_i) = \prod_{j=1, j\neq i}^{M} (y_i - y_j),$$

$$w_{ij}^{(n)} = \begin{cases} n\left(w_{ij}^{(1)} w_{ii}^{(n-1)} - \dfrac{w_{ij}^{(n-1)}}{x_i - x_j}\right), & i \neq j \\ -\displaystyle\sum_{k=1, k\neq i}^{N} w_{ik}^{(n)}, & i = j \end{cases}$$

$i, j = 1, 2, \dots, N$ (eq. 8)

$n = 2, 3, \dots, N - 1$

$$\bar{w}_{ij}^{(m)} = \begin{cases} m\left(\bar{w}_{ij}^{(1)} \bar{w}_{ii}^{(m-1)} - \dfrac{w_{ij}^{(m-1)}}{y_i - y_j}\right), & i \neq j \\ -\displaystyle\sum_{k=1, k\neq i}^{M} \bar{w}_{ik}^{(m)}, & i = j \end{cases}$$

$i, j = 1, 2, \dots, M$ (eq. 9)

$m = 2, 3, \dots, M - 1$

After these coefficients have been determined, the coefficients of the second and higher derivatives can be derived from the coefficients of the first-order derivative. Since the GDQ method uses the same form for different derivatives at different grid points (as long as all the grid points are known), one do or for loop will suffice for the discretization at all the grid points. This is one of the aspects that allow the GDQ method to use much less computational resources than the low-order finite difference method. [11]

The GDQ method's accuracy can be shown by comparing it to other methods. As table 1 shows, when the GDQ method is compared against a second-order central difference scheme (CD) and a second-order upwind QUICK scheme (QUICK), the GDQ method is very accurate. The CD method uses a 65x65 grid, the QUICK method uses an even finer 80x80 grid, and the GDQ method uses a coarse 15x15 grid. The methods were compared by looking at the maximum and minimum absolute values of the stream function, denoted by ψ_{min} and ψ_{max}; and each method was tested for 3 cases. Case A is a forced convection problem where the flow is driven by the rotation of the crystal. Case B is also a forced convection problem, but in case B the flow is driven by the opposing rotations of the crucible and crystal. Case C is a natural convection problem.

[11] Ibid, 429

Table 1: A comparison of stream function values using different methods; for different cases.

	Method	Mesh Size	ψ min	ψ max
Case A	GDQ	15x15	-2.2234×10^{-1}	5.4623×10^{-6}
	CD Scheme	65x65	-2.3447×10^{-1}	1.5642×10^{-6}
	QUICK Scheme	80x80	-2.1724×10^{-1}	4.0630×10^{-6}
Case B	GDQ	15x15	-6.8088×10^{-2}	1.1722×10^{-1}
	CD Scheme	65x65	-5.0203×10^{-2}	1.1796×10^{-1}
	QUICK Scheme	80x80	-4.4332×10^{-2}	1.1722×10^{-1}
Case C	GDQ	15x15	-7.4951×10^{-3}	2.8316×10^{1}
	CD Scheme	65x65	-1.1936×10^{-3}	2.8437×10^{1}
	QUICK Scheme	80x80	-5.7979×10^{-4}	2.8409×10^{1}

The GDQ method is very close to the other two methods when computing the maximum values of the stream function (ψ_{min} for case A, ψ_{max} for cases B and C). But when the GDQ method is used to calculate the minimum values of the stream function (ψ_{max} for case A , ψ_{min} for case B and C), there are some small discrepancies. However, these differences are negligible because the stream function's minimum absolute value is fairly small.[12]

As shown above, the GDQ method will work well for modeling the stream function. But to accurately simulate heat transfer and oxygen segregation, it is necessary to model the turbulent convection in the melt. Thermal capillary models of the Czocheralski growth can determine conductive and radiative heat transfer in the crystal, melt, and surrounding components. However, the accuracy of the thermal capillary model depends on the accuracy of the model of the convection in the melt, among other things.[13] The three possible models that will be examined are based on the k-ε turbulence model (k is the kinetic energy, ε is the dissipation function). These

[12] Ibid, 432

[13] Brown, "Comparison of three turbulence models for simulation of melt convection in Czocrhralski crystal growth of silicon" (Journal of Crystal Growth 205 no. 1), p 71-72_

methods rely on single-point turbulence models, which are based on approximations of Reynolds average equations of momentum, mass, heat and species transport. Reynolds average equations are solved using approximations of couplings between the time-varying components of these variables.[14] The three *k*-e models vary in their approach to the description of the flow around solid boundaries.

Accurate flow modeling requires the correct coupling between the turbulent flow and the layers near the walls where there is a thin, viscous layer. The *k*-e models that will be examined vary in the way they model the flow near these walls. The first *k*-e method (WF) uses wall functions that are constructed from the structure of the turbulent shear flow to produce the boundary conditions along the surface. The second method (TL) uses a two layer model that uses a one equation model for the flow near walls instead of the wall functions. The third method (JL) uses a low Reynolds number *k*-e model that is designed to eliminate the need to use special models for the conditions near the wall.[15] The methods will be compared for both rotational and buoyancy driven flow.

The WF method hopes to avoid the issue of the transition from the turbulent core to the viscous wall layer by modeling the junction with simple models valid for parallel shear flow. These models then can be matched to the core flow calculated by the *k*-e model. However, the wall function is not necessarily accurate. In similar problems, simulations with wall functions have over-predicted the wall heat transfer by as much as 50%. Also, the wall function's accuracy is sensitive to the distance of

---

[14] Ibid, 73
[15] Ibid, 73-74

the closest grid point to the wall, and the wall function assumes a one-dimensional averaged motion near the wall when in fact it is two-dimensional.[16]

The TL method uses an algebraic stress model of the standard *k*-e model of the core flow, and a one equation, simple mixing model with a low Reynolds number near the wall regions. Calculations using a similar set up gave promising results using the TL method.[17] The JL method is the third and final method that will be examined. The JL method uses low Reynolds number forms of the *k*-e model that will hopefully produce smooth transitions between the turbulent core and the flow along the wall.[18]

These three methods were used with the finite volume method to produce results. The grid that was used for the TL and JL models had 49 control volumes in the radial direction and 69 controls in the z-direction. The mesh refinement in the z-direction is necessary because of the need for mesh refinement on the crystal's surface and the bottom of the crucible. The mesh for the WF method is similar, but left out the mesh refinement near the boundaries, leaving the WF method with 49 controls in the radial direction and 59 controls in the z-direction. After running the experiment, shortfalls in he WF and the TL method were found. As mentioned before, the WF method is sensitive to the placement of the first grid point to the wall. Changing this distance by a factor of three was enough to increase the variation in the turbulent viscosity by 20% and the stream function by 7%.[19] The problem with the TL model is that it uses a one-dimensional model for the near-wall conditions. With

---

[16] Ibid, 77
[17] Ibid. 77
[18] Ibid, 78
[19] Ibid, 79

increasing rotation rates, the flow becomes similar to a pure shear driven motion in the near-wall region. While the error in the TL model is less than that of the WF model, it should be noted and taken into consideration when choosing which method to use.[20]

For the rotationally driven flow, the WF method fails because the first grid point must be set too far from the wall. The placement of the grid point results in wiggles in the velocity field near the crucible, which is an intrinsic problem to the WF model. The TL model works well, but does not predict the flow as accurately as the JL model.[21] However, the JL model is quite good. Where the JL model predicts nearly laminar flow, the stream function of the laminar solution is smooth, and there are small wiggles in the stream function's solution in the region where the JL model predicts weak turbulence.[22] For buoyancy driven flow, all models predicted the same patterns for the stream function and temperature fields. The TL model is the most incorrect, whereas the WF and JL methods produce similar, accurate results. Upon closer inspection, however, the WF model predicts a more turbulent flow than the flow that actually exists, whereas the JL method is still very accurate.[23]

The comparison of these three models points to some general conclusions. First, in all three models, as the rotation rate increases the flow becomes highly turbulent; and all three models produce very similar results for the core flow. But near the boundaries, the viscous force is more important than the turbulent force, because turbulence is weak near the boundaries. Both the WF and the TL models fall

[20] Ibid, 80
[21] Ibid, 80
[22] Ibid, 83
[23] Ibid, 83

short in how they deal with their representation of the boundary layer near the walls. There is an intuitive connection between the results of the JL model and the predictions of laminar flow where the flow is weak; therefore the JL model is the best model to use.[24]

Results:

The following figures are the frames of the video with the particles' paths traced out on them. Notice that many of the paths traced in the following pictures appear to be roughly the same length. This is because the particles can only be seen while they are illuminated by the plane of light, and the plane of light has a set width. While the paths of the particles are approximately the same length, the time that it took the particles to travel that length is different. Figures 5 through 8 show the particles' movement on the surface of the water, whereas figures 9 through 13 show a view from the bottom of the ingot.

Figure 5 shows the path of a particle taken while the ingot was moving at about 1 revolution per second, which is roughly 0.24 m/s along the ingot's outer edge. The linear velocity of the particle is 0.032 m/s, roughly 1/8th of the speed of the ingot. The angular velocity of the same particle should scale with the linear velocity, and is approximately 48°/s.

[24] Ibid, 89

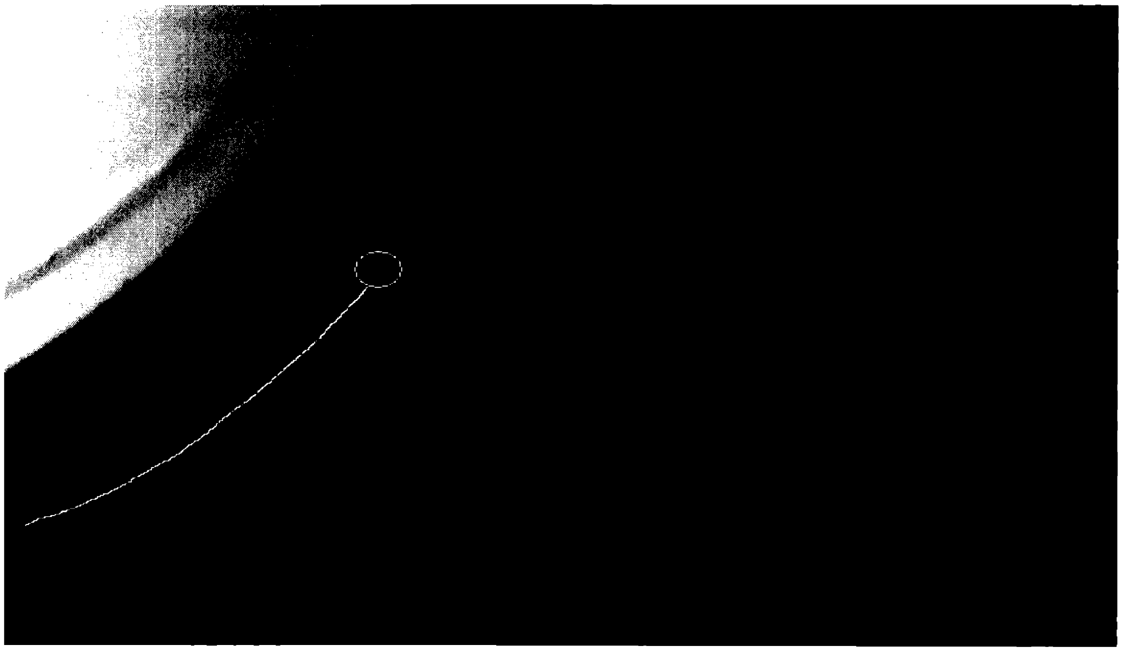

Figure 5: The path of a particle (the particle is circled). The path is 4 cm long, the particle traveled that distance in 1.25 seconds.

Figure 6 shows a zoomed image taken from the same vantage point as figure 5. Figure 6 is taken while the ingot spinning at 2.5 revolutions per second, which is 0.60 m/s along the ingot's circumference. The 2 paths shown in figure 6 are very similar to each other; even almost parallel to each other at each point. This suggests that the flow at roughly 3 cm from the ingot is laminar since there is very little perturbation of 2 separate yet physically close paths. The particles travel about 1.5 cm over the course of a third of a second. Therefore the particles have a linear speed of about 0.045 m/s, which is proportionately slower than the particles in figure 5. In figure 5, the ingot's outer edge was traveling at a linear speed of 0.24 m/s, while the particles were at 0.032 m/s; roughly $1/8^{th}$ the ingot's speed. However, the particles in figure 6 are traveling at about 1/13th the speed of the ingot. As the ingot moves faster, the ingot glides through the water more and more and drives the fluid flow less.

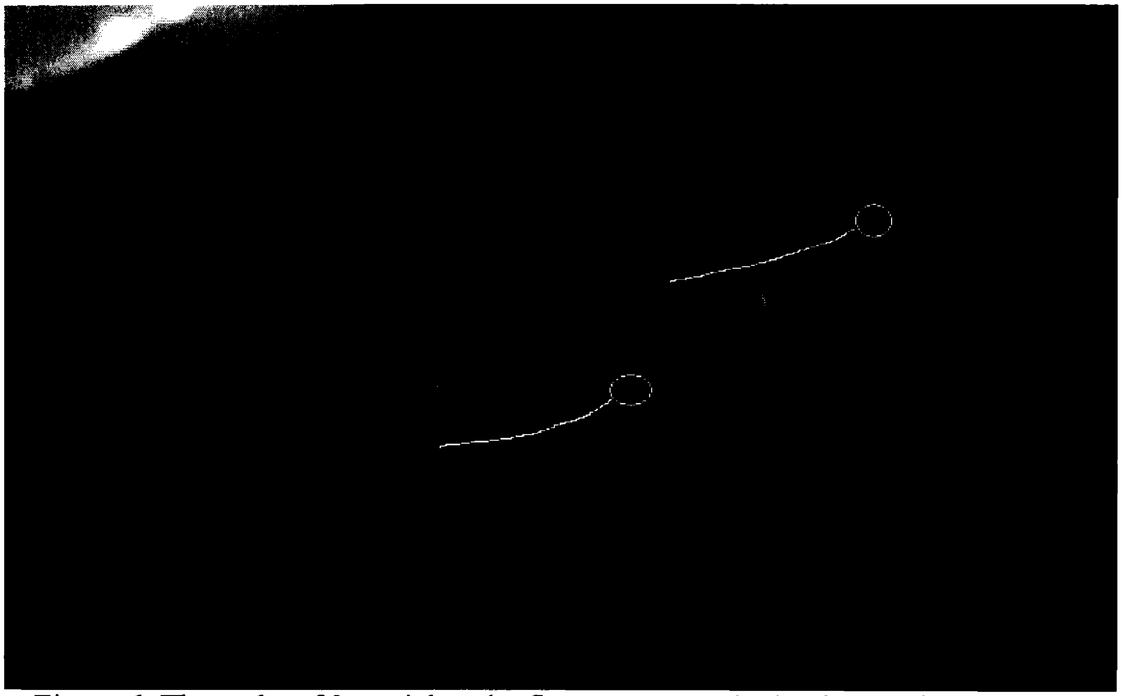

Figure 6: The paths of 2 particles, the flow appears to be laminar and the particles have an angular velocity of approximately 67°/s.

Figure 7 shows another shot from a similar vantage point. In figure 7, the ingot is moving at the same speed as in figure 6 (900°/s, 0.60m/s along the circumference). The particle moves about 1 cm in 0.2 seconds, giving a linear velocity of 0.05m/s. This velocity is close to the velocity of the particles in figure 6, yet is slightly faster. One reason for the increase in velocity could be that the particle in figure 7 is much closer to the ingot and therefore travels at a slightly faster rate. The particle is traveling at an angular velocity of 75°/s, compared to the ingot's angular velocity of 900°/s.

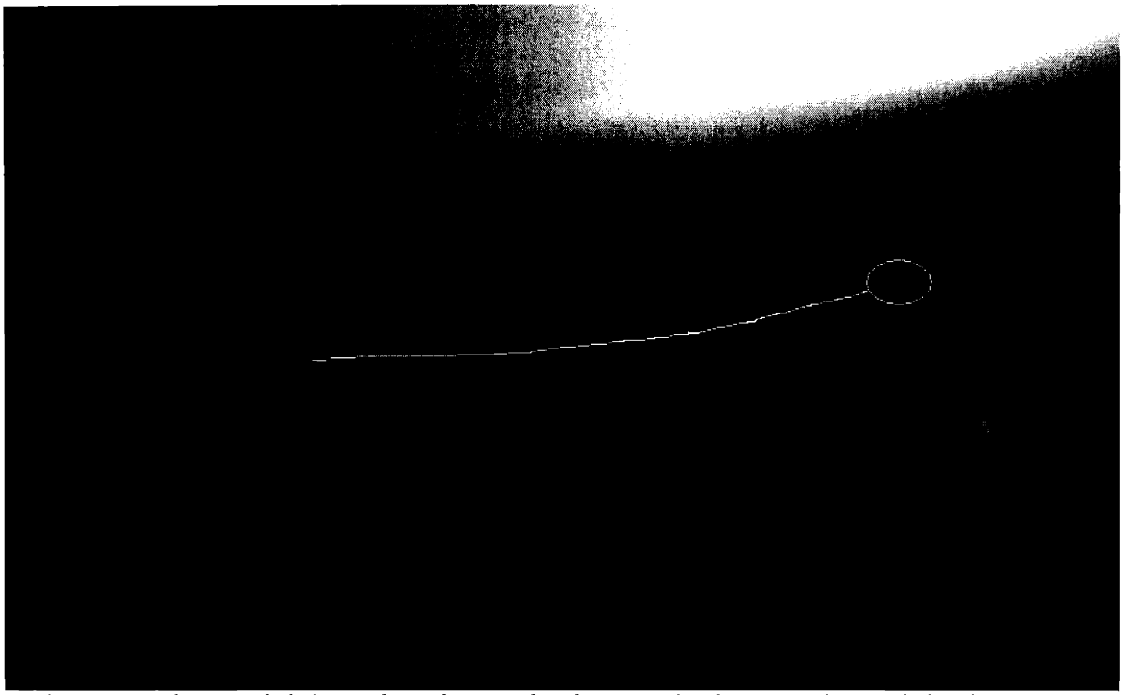

Figure 7: The particle's path as it travels close to the ingot. The path is about 1 cm long, the particle is traveling at a linear speed of 0.05m/s, with an angular velocity of 75°/s.

Figure 8 is very similar to figure 7. Figure 8 is almost the exact same camera angle, yet zoomed in and the ingot is moving slower. Just as in figure 5, in figure 8 the ingot moves at 1 revolution per second (360°/s), which is a linear velocity of 0.24 m/s at the ingot's circumference. In figure 8, the paths of the particles are 0.4 cm long, and the paths again look laminar, and it took the particles 0.2 seconds to travel this distance. This gives a linear velocity of 0.02m/s, which translates to an angular velocity of 30°/s.

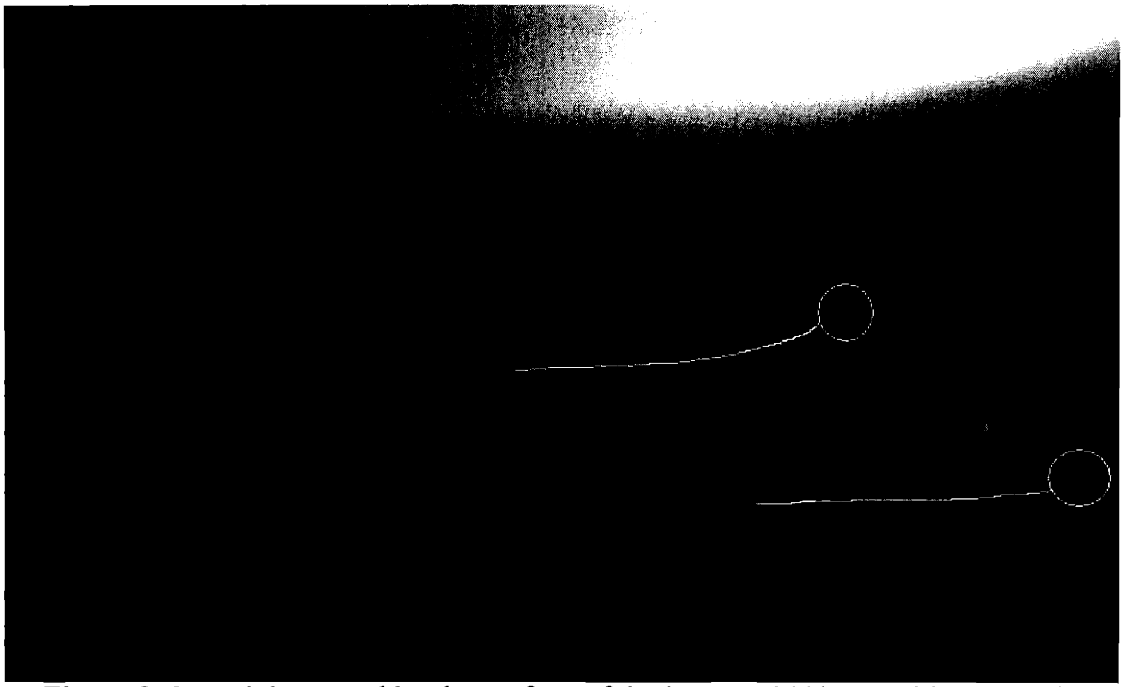

Figure 8: 2 particles travel by the surface of the ingot at 30°/s, roughly 0.02 m/s.

More importantly, the similar paths of the particles in figures 6 and 8 suggest that on the surface, the flow is laminar. While the lack of turbulence seems distressing and could result in dendrite formation, it is important to remember the speed of the ingot. Even in figure 7, where the particles are moving the fastest relative to the ingot out of figures 5-8, the particles are still only moving at 0.05m/s linearly and only have an angular velocity of 75°/s. These speeds are an order of magnitude slower than the speed of the ingot, which, in figure 7, is traveling at 900°/s and 0.60 m/s. While the figures do not necessarily show a turbulent layer around the edge of the ingot on the surface, the pictures do indicate a lot of shear around the edge. The ingot is moving at least ten times faster than the fluid around it, this large discrepancy in speeds could create enough shear to prevent the formation of dendrites.

Figure 9 shifts the focus to the bottom of the ingot. Now that the camera is looking into the water (as opposed to figures 5-8, where it was focused on the surface of the water), the radial and z-direction velocities can be determined. The paths can be broken into their r and z components, the size of those components can be determined, and by using the particles travel time the velocities can be computed. The ingot was spinning at 900°/s in figure 9. The radial component (the horizontal component in this picture) is 1.6 cm long, and the z-component is .75 cm long. The particle took 0.5 seconds to move that distance. Therefore, the velocity in the r direction is 0.032 m/s, and the velocity in the z direction is 0.015 m/s.

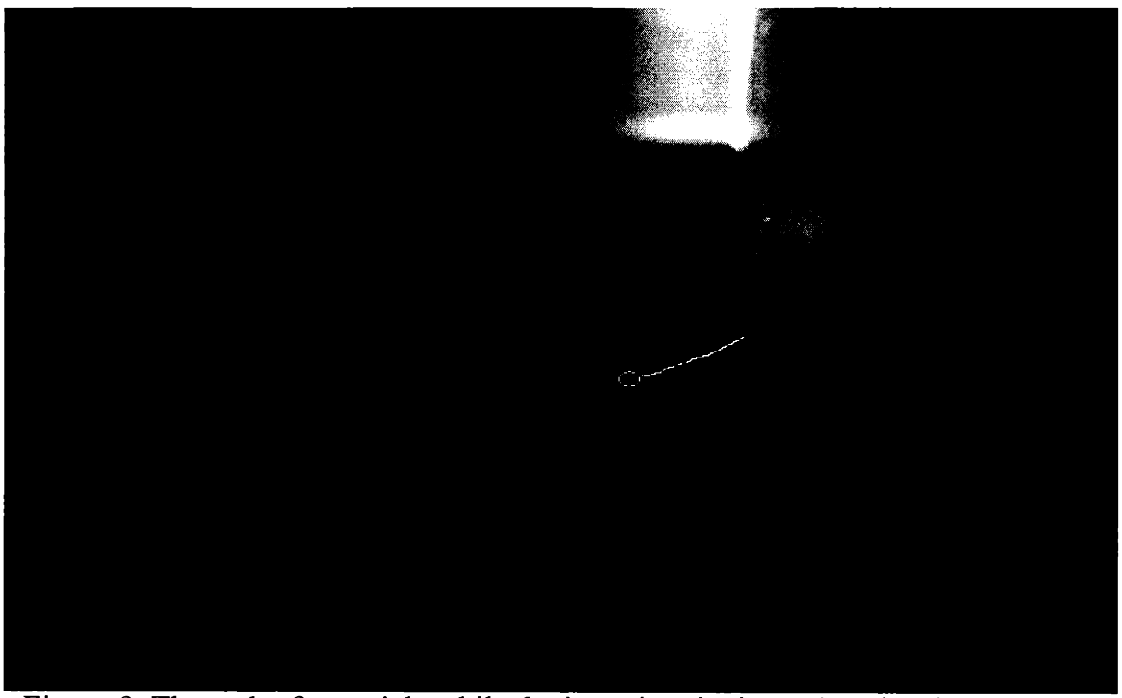

Figure 9: The path of a particle while the ingot is spinning at 900°/s. The particle is moving with a radial velocity of 0.032 m/s and a z-direction velocity of 0.015 m/s.

Figure 10 shows one of the particles that is not under the ingot traveling up towards the surface. The ingot is moving at the same speed that it was in figure 9. The velocities in the r and z directions from figure 9 are slower than the linear velocities of the particles on the surface in figures 6 and 7, where the ingot is moving at the same speed. This could create a drawing flow in the water where the slower moving particles are drawn up toward the surface because the particles are moving faster on the surface.

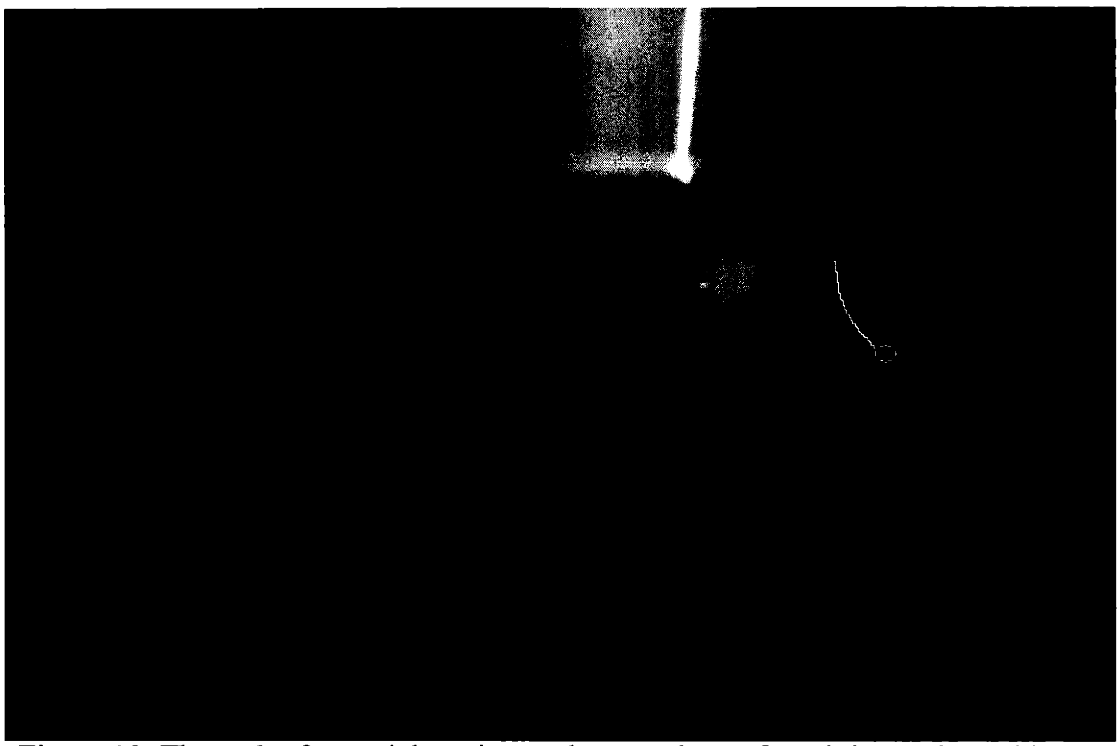

Figure 10: The path of a particle as it travels up to the surface, it is moving with a z-velocity of 0.042 m/s

The z component of the path in figure 10 is much larger than the r component. The particle travels 1.25 cm in the z-direction, whereas it only travels 0.6 cm in the r direction. The particle takes one third of a second to travel its path, giving it a z velocity of 0.042 m/s and a radial velocity of0.02 m/s. As mentioned before, the particle is moving faster than the particle in figure 9.

Figure 11 is interesting. It shows that there are two layers of flow occurring near the bottom of the pipe. The layer shown in figure 9 is present in figure 11;

where particles near the bottom of the ingot are flowing up to the surface. But figure 11 shows another layer too. Further away from the bottom of the ingot, there is a layer of flow that is moving down towards the bottom of the tank. It looks as if there is a circular motion occurring, where particles close to the bottom of the ingot are brought up to the surface of the tank, then as the particles move away from the ingot they are caught in a flow that takes them back down towards the bottom of the tank..

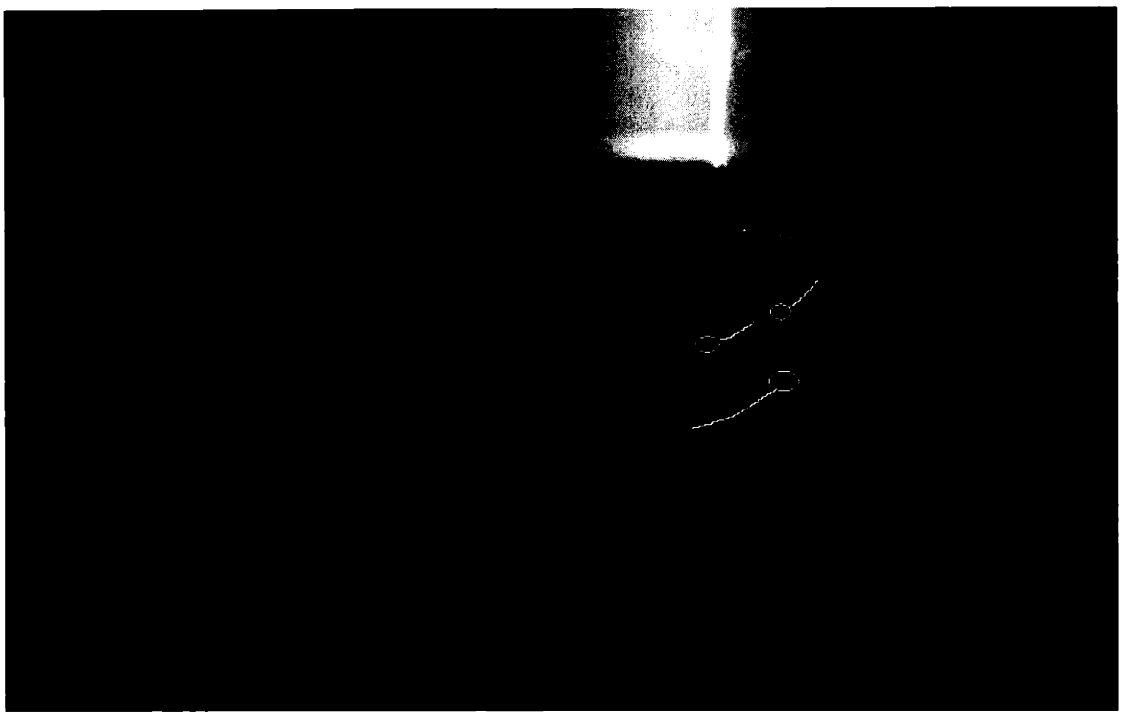

Figure 11: The particles rise up, move away from the ingot and flow back down towards the bottom of the tank.

In figure 11 the ingot is spinning at the same speed as in figures 9 and 10. The two particles going up have almost the same path length; a 0.7 cm vertical travel and a 0.4 cm radial travel. The particle that is going towards the bottom of the tank has a longer path; a 1.3 cm radial travel and a 0.8 cm vertical path. The particles covered this distance in 0.4 seconds. These path lengths correspond to z velocities of 0.0175 m/s for the particles traveling up and 0.02 m/s for the particle going down. The radial velocities are 0.01 m/s for the particles that are traveling away from the center of the ingot and 0.0325 m/s for the particle that is traveling towards the center of the ingot. Figures 9 – 11 have examined the bottom of the ingot at high speed (900°/s), now figures 12-13 will examine the same area at 360°/s.

Figure 12 is similar to figure 10, yet figure 12 shows two particles moving up towards the surface and in figure 12 the ingot is spinning much slower.

Figure 12: Two particles rise towards the surface. The particles have the same vertical travel, as well as the same horizontal path, but the horizontal paths are in opposite directions.

The vertical path is 0.6 cm for both particles, the horizontal path is 0.15 cm for both particles (although the particles are moving towards each other). This occurred over 0.7 seconds, giving the particles a velocity of 0.008 m/s in the z-direction and 0.002 m/s in the radial direction. The particles are moving much more slowly because the ingot is rotating much slower too.

Figure 13 shows a particle moving along the bottom of the ingot. The particle has no z-component, it is only moving horizontally. The path is 1 cm long, and takes 0.9 seconds to travel the path. Therefore, the particle's radial velocity is 0.011 m/s; its z component of velocity is 0 m/s.

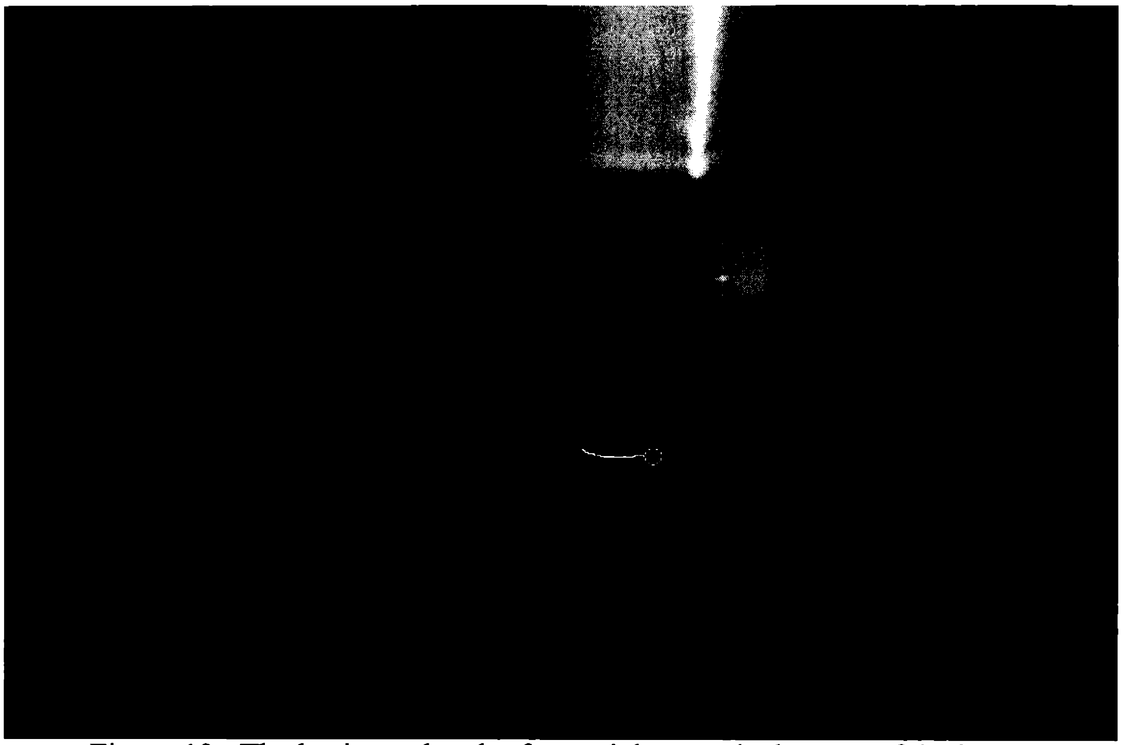

Figure 13: The horizontal path of a particle near the bottom of the ingot.

The lack of a z component to the velocity suggests that near the bottom of the ingot, if the particle is not very close to the ingot, it is not pulled back up along the bottom of the ingot to the surface.

Conclusions and Recommendations:

The SOMERC Process could revolutionize the way titanium is made. A lower operation cost combined with a superior final product make the SOMERC process much more promising than the current Kroll process. In order for the final ingot to be of the highest possible quality, the speed of the ingot's rotation and the ingot's interaction with its surrounding fluid must be controlled. If there is not enough shear across the surface of the ingot, the possibility of dendrite formation increases. This occurs because of the Mullins-Sekerka instability. By having a large shear across the bottom of the ingot, there will be a thinner boundary layer, and perturbations could move and decay instead of growing into dendrites. Of the two speeds that were tested, there was more shear across the surface of the ingot when it was spinning at 2.5 revolutions per second.

When the ingot was spinning at 1 revolution per second, or 360°/s, the linear speed at the edge of the ingot was 0.24 m/s, and it created an average linear speed on the surface of 0.026 m/s. Beneath the surface of the water, the ingot created flows that averaged to 0.01 m/s in the radial direction and 0.008 m/s in the z-direction. When the ingot was spinning at 2.5 revolutions per second (900°/s), it had a linear speed at its edge of 0.60 m/s. On average, it created linear surface velocities of 0.048 m/s. Under the surface of the water the ingot's rotation made an average radial velocity of 0.022 m/s, and an average velocity of 0.02 m/s in the z-direction.

Since the rotation rate that creates the most shear is desired, whichever speed creates the largest discrepancy between the ingot's speed and the particles' velocities is the speed that should be examined further. At the higher speed, the ingot is moving 2.5 times as fast as it is at the lower speed. The water on average is only moving 1.8 times as fast on the surface at the higher speed. Under the surface, the water moves 2.2 times as fast in the radial direction and 2.5 times as fast in the z-direction at the faster rotation rate. Therefore, at the faster rotation rate, there is a bigger difference between the ingot's rotation rate and the surface and underwater radial speed of the flow. There is no difference in the ratio between the ingot's rotation speed and the flow in the z-direction at the two speeds. For a higher shear between the ingot and the surrounding fluid, the 900°/s rotation speed is better than the 360°/s rate.

For further study of the fluid flow, it is recommended to run the ingot at least at 900°/s. Unfortunately, only so much can be done with a video camera, a plane of light and some TiO_2 particles. Using a particle image velocimetry system in conjunction with the GDQ mesh and the JL system for modeling the coupling between the turbulent and non turbulent layers, a more accurate picture of the flow can be developed. If the SOMERC process can be developed and put into practice, the cost of titanium will drop and titanium can be used for many more applications; for titanium oxide is very abundant. The lower cost of titanium may even inspire new uses of the metal that were cost-prohibitive when titanium was refined through the Kroll process. Hopefully the SOMERC process will achieve its full potential in years to come.

Acknowledgements

The author would like to thank Josh Weaver and Professor James Bales who work in the Edgerton Center. Josh and Professor Bales gave the author advice on how to set up my light boxes, as well as clued the author in on the inner workings of the camera he used. The author would also like to thank Salvatore Scatturo. Sal lent his Canon Optura 300 to the author. The Canon took the beautiful videos and provided the excellent images seen in this report. Without Sal's generosity in lending his camera to the author, it would have been much harder to perform the experiments and analyze the data. Finally, the author would like to thank Professor Adam Powell, who guided and helped the author from day one until the thesis was done. Professor Powell never hesitated to offer his assistance and support throughout the entire thesis project, it would have been infinitely harder to conduct the experiments and write this thesis without him.

References

Brown, "Comparison of three turbulence models for simulation of melt convection in Czocrhralski crystal growth of silicon" (Journal of Crystal Growth 205 no. 1), pages 71-83

Chew, "An efficient approach for numerical simulation of flows in Czochralski crystal growth" (Journal of Crystal Growth 181, no. 1), pages 427-432

Crowley, "How to Extract Low-Cost Titanium" (Advanced Materials and Processes 161, no. 11), page 27

Faller, "Titanium alloy to be placed in Japanese automobiles" (Advanced Materials and Processes 160, no. 1), page 15

Kirchain, Randolph. *The role of Titanium in the Automobile: Understanding the Economic Implications of Three Emerging Technologies.* Technical Report, Camanoe Associates, USA, July 2002.

Merton Flemings, Raul A. Martinez, private conversation

Powell, Adam. "Solid Oxide Membrane Electrolysis with Rotating Cathode (SOMERC), a Low-Cost Process for Commercial-Purity Dense Titanium," MIT Technology Licensing Office Disclosure Report, January 9, 2003

About the Author

Christopher Kinney is a senior in Materials Science and Engineering at the Massachusetts Institute of Technology. He will be graduating in June of 2004, and plans to attend the University of California at Berkeley in the fall to obtain a master's degree in Materials Science and Engineering. Chris works part time during the school year teaching high school students math and science; he also works for a fledgling electrical connector company started by MIT graduates. Other than Materials Science and Engineering and teaching, his passions include motorcycles, swimming and skiing. Chris works during the winter at Heavenly Ski Area, in South Lake Tahoe as a ski patroller. After finishing his education at U.C. Berkeley, Chris plans to become a teacher at the high school or college level, teaching math, chemistry and materials science.